

Quantifying the Features of an Amorphous Solid’s Local Yield Surface

Spencer Fajardo,¹ Paul Desmarchelier,² Sylvain Patinet,³ and Michael L. Falk^{1,4,5,6,7}

¹*Materials Science and Engineering, Johns Hopkins University, Baltimore, MD USA*

²*Sorbonne Université, CNRS, Physico-chimie des Électrolytes et Nanosystèmes Interfaciaux, PHENIX, 75005 Paris, France*

³*PMMH, CNRS, ESPCI Paris, Université PSL, Sorbonne Université, Université Paris Cité FRANCE*

⁴*Mechanical Engineering, Johns Hopkins University, Baltimore, MD USA*

⁵*Physics and Astronomy, Johns Hopkins University, Baltimore, MD USA*

⁶*Hopkins Extreme Materials Institute, Johns Hopkins University, Baltimore, MD USA*

⁷*Data Science and AI Institute, Johns Hopkins University, Baltimore, MD USA*

(Dated: March 19, 2026)

In two-dimensional Lennard–Jones glasses, mechanical probing reveals that local yield surfaces are dominated by regions with a positive second derivative of the yield stress with respect to the loading angle. Each feature corresponds to a shear transformation zone and a characteristic non-affine displacement field at yield. Most features are well described by a combined Schmid–Mohr–Coulomb criterion parameterized by a weak-plane orientation, a critical stress, and a pressure sensitivity. The resulting parameter statistics clarify how the onset of plastic flow is governed by the population of discrete yielding features encoded in the amorphous structure.

Amorphous solids are a broad class of materials that exhibit non-crystalline solid structure [1] often produced by rapidly cooling a liquid or depositing a vapor so as to inhibit the kinetics of crystallization [2]. Understanding the mechanical behavior of these materials beyond the elastic regime remains hindered by an inability to rationalize plastic response in terms of distinct features of the amorphous structure [3–9]. Plasticity in amorphous solids is thought to be mediated by shear transformation zones (STZs) [10], discrete local structural features that are susceptible to rearrangement under shear and act as flow-defects. An important question that remains is how these STZs embedded in the material’s structure control the yield response at the nanoscale. In this work, we link the nanoscale structure of a metallic glass to its plastic behavior by adapting continuum-mechanical concepts to the nanoscale.

In continuum mechanics, the concept of a yield surface is commonly used to describe the yielding conditions of a material under complex loading conditions [11–14]. The yield surface specifies the stress conditions that trigger plastic flow, defining an envelope within which the material behaves elastically. We extend this idea from continuum mechanics to the nanoscale to establish a direct connection between the yield stress concept and the atomic-scale physics of the STZs that control plasticity.

Here we show that most positive-curvature segments of the local yield surface can be mapped one-to-one to STZ-like rearrangements and fitted by a Schmid–Mohr–Coulomb form, enabling parameter statistics vs quench rate. We describe the system we use as a model of amorphous solids and the nanoscale mechanical probing technique used to induce plasticity. By deploying this technique, we measure stress at the point of plastic onset to determine the angular and pressure dependence of these plastic events. Finally, we show that the yielding behavior of the model amorphous solid can be de-

scribed by a yield criterion that incorporates aspects of the Schmid and Mohr–Coulomb yield criteria. This form is used to collect statistics on physical parameters that characterize the material’s yielding behavior as a function of the preparation protocol. These results show, from a unitary flow-defect perspective, that yield stress and pressure sensitivity increase as glass is quenched more deeply.

Methods— We study the local plastic response of a simulated two-dimensional, binary Lennard–Jones (LJ) glass-forming system [15–17]. Glass structures are generated using the procedure described in Ref. [18]. The LJ pair potential cutoff with energy and force shifting is adapted from Wahnström [19]; details of the smoothing and shifting procedure are provided in the Supplemental Material [20].

Each system consists of 15,625 atoms composed of two different species, designated as Large (L) and Small (S), where the number of large atoms (N_L) and the number of small atoms (N_S) is given by the ratio $N_L : N_S = (1 + \sqrt{5}) : 4$, both with mass $m = 1$. All quantities are reported in reduced Lennard–Jones units: length is measured in units of a_{SL} the distance at which an S and an L atom have zero potential energy; energy is measured in units of the bond energy between S and L atoms, ϵ_{SL} ; and time is measured in units of $\tau = a_{SL}\sqrt{m/\epsilon_{SL}}$. The zero-potential-energy distances between like atom types are $a_{LL} = 2\sin(\pi/5)a_{SL}$ and $a_{SS} = 2\sin(\pi/10)a_{SL}$ respectively. The bond energies between two like atoms are $\epsilon_{LL} = \epsilon_{SS} = 0.5\epsilon_{SL}$. In this system, the glass transition temperature is known to be approximately $T_g \approx 0.325\epsilon_{SL}/k_B$ [15]. After initializing the atoms with an initial density of $1/V_{atom}$, where $V_{atom} = 0.976a_{SL}^2$ and imposing periodic boundary conditions, the system is heated to a melting temperature $T_m = 2T_g$ using a Nose–Hoover thermostat and equilibrates at this temperature before it is cooled down

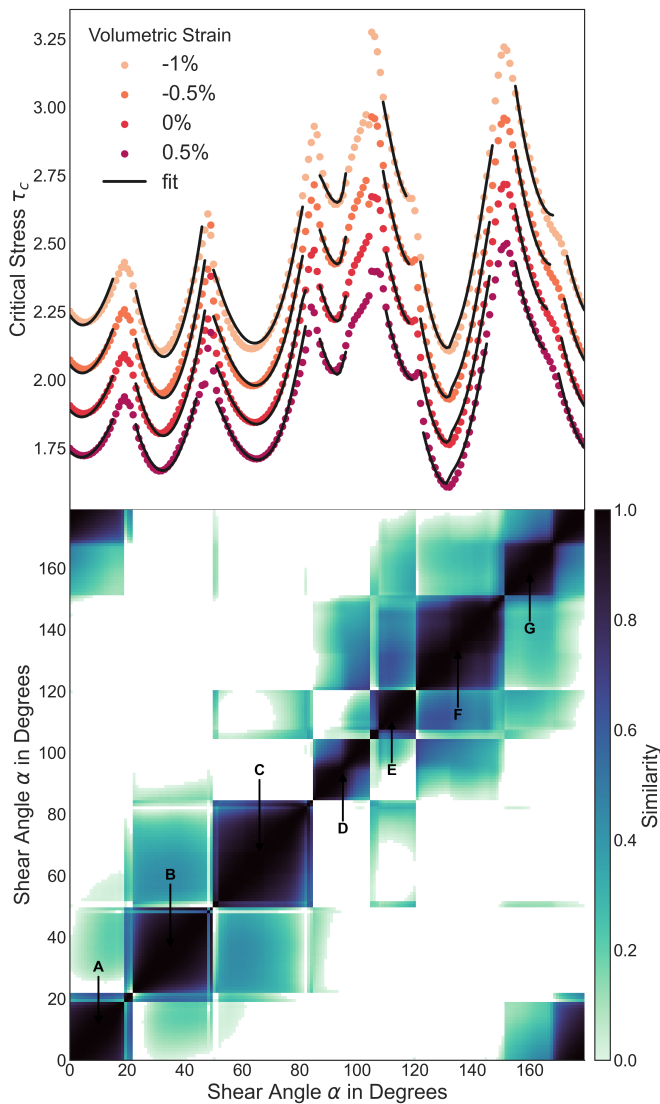


FIG. 1: Top: Critical stress as a function of shear angle, defining a local yield surface. Symbols and lines correspond, respectively, to the atomistic data and their fit (Eq. 2); colors indicate the volumetric-strain conditions. Bottom: Similarity metric (Eq. 3) quantifying the alignment of plastic non-affine displacement fields; regions along the diagonal are labeled A–G.

to a final temperature $T_f = 0.092T_g$. Slower quenching rates result in glasses that are more deeply quenched with lower potential energies that are typically harder and more brittle than more quickly quenched glasses [1, 4, 9]. We study glasses prepared at four cooling rates: $7.632 \times 10^{-5}T_g/\tau$, $7.632 \times 10^{-6}T_g/\tau$, $7.632 \times 10^{-7}T_g/\tau$, and $8.885 \times 10^{-8}T_g/\tau$. We will refer to these glass preparation methods as G1, G2, G3, and G4, where G1 is the fastest cooling rate, and G4 is the slowest.

The local yield stress (LYS) method systematically measures the shear stress at which a local region of a

material yields when subjected to incrementally increasing shear strains [21–23]. Locations in a glass structure with low LYS have been shown to correspond to sites of plasticity upon remote loading [21, 23]. Here, we employ the LYS procedure to calculate the critical stress τ_c , which is the shear stress in the loading direction at the point of yielding, by applying athermal quasi-static shear (AQS) [24, 25] to circular regions of the system $10a_{SL}$ in radius. Two different subregions are defined within this circle: an outer annular region from $5a_{SL}$ to $10a_{SL}$ within which the atoms will be constrained to shear, and an inner region from the center to $5a_{SL}$ free to mechanically equilibrate as the outer region is deformed. The sample is affinely deformed in pure shear strain increments of $\Delta\gamma = 10^{-4}$. Between each strain step, the positions of the atoms in the inside region are relaxed to a minimum energy configuration via a conjugate gradient scheme. This process is repeated until the stress in the loading direction decreases from one step to the next, signaling plastic deformation. At this point, the two-dimensional stress state at the onset of instability $\bar{\sigma}^c$ is recorded. Finally, the critical shear stress is computed as

$$\tau_c = (\bar{\sigma}_{oi} : \hat{S}_{ij}), \quad (1)$$

where \hat{S}_{ij} is a unit tensor in the direction in which the shear strain is applied.

Results and Analysis— We use the above-described method to construct yield surfaces of various circular regions from our system. This is done by probing the critical shear stress over a range of angles, thereby mapping out the maximum elastic stress attainable before the onset of plasticity. Figure 1 shows a plot of τ_c as a function of shear angle α for a particular region of our glass. We observe that the yield surface shown in Figure 1 is composed of wells, as one would expect in materials governed by a yield criterion wherein slip occurs along weak planes along particular shear directions.

To confirm the hypothesis that the yield surface can be decomposed into distinct regions corresponding to the activation of particular STZs with characteristic shear directions, we divide the yield surface into regions of positive and negative curvature. Positive curvature segments constitute 69.25% of all yield surfaces. We then seek to associate a distinct STZ with each of these regions. We hypothesize that the negative curvature cusps correspond to transitions between activating one distinct STZ and another as the angle of applied strain is varied.

Previous work has shown that the yielding response in models of metallic glasses is pressure-dependent, consistent with the Mohr-Coulomb yield criterion [13, 26–28]. To describe the orientation and pressure dependence of the plastic response due to the activation of differently oriented STZs with a variety of critical stresses, Lerbinger [29] developed a two-dimensional yield criterion that

incorporates elements of both the Mohr-Coulomb and Schmid law of the form

$$\tau_c(\alpha) = \frac{\tau_0 - \phi p^c}{\cos(2(\theta - \alpha))} - \frac{\sigma_{yy}^c - \sigma_{xx}^c}{2} \tan(2(\theta - \alpha)). \quad (2)$$

This criterion is meant to provide a piecewise continuous description of the portion of the yield surface associated with a single STZ. Here, the critical stress is a function of the shear angle α and depends on the orientation of the STZ, θ , the intrinsic critical stress, τ_0 , which is the minimum shear required to activate the STZ in the absence of pressure, and the pressure dependence of the plastic response, ϕ . In two dimensions, the hydrostatic pressure at the point of yielding is $p^c = -(\sigma_{xx}^c + \sigma_{yy}^c)/2$. The pressure dependence ϕ is typically negative, indicating that the critical stress increases under pressure [26, 27]. An example of this behavior is observed in data from differently strained samples as shown in Figure 1. For each sample, we generate additional pressure conditions by applying the same incremental shear process as in the LYS method, but with an applied hydrostatic strain. The second term on the right-hand side of Eq. 2 takes into account the anisotropic response of the material to stress, where $\sigma_{yy}^c - \sigma_{xx}^c$ represents the orthogonal shear stress projected along θ at the point of yielding.

To determine the parameters θ , τ_0 , and ϕ , we associate positive-curvature regions spanning overlapping angular ranges across multiple volumetric strain conditions. Regions observed under only a single pressure state are excluded, since the yield-criterion parameters cannot be uniquely identified from a single condition. Regions spanning less than 5° of the yield surface are also excluded. Parameters are obtained by nonlinear least-squares fitting of Eq. 2 [30]. Figure 1 shows the resulting fits. We find that 92.65% of fitted points exhibit deviations of less than 5% from their measured values.

By sampling 144 independent regions extracted from each of four glass models, we collected statistics on 4726 positive curvature regions as shown in Figure 2 and in Table I. This represents an average of 8.2 STZs per region accounting for between 82–84% of the positive curvature regions of all samples. For more details on the percentage of yield surfaces fit, and the average error in fits see Supplemental Materials.

We analyze the cumulative distributions for both τ_0 and ϕ excluding outliers. Statistical tests show that the distributions are consistent with normality. We observe a systematic trend that glasses produced at lower cooling rates exhibit a 27.8% higher average τ_0 , confirming our expectations [31–34]. The average ϕ shifts 17.3% towards more negative values as the cooling rate decreases, indicating that the pressure dependence of the yield stress increases in magnitude as the quench rate decreases. Both of these parameters exhibit a logarithmic relationship to the quench rate, in line with the literature (See Supplemental Material). [31–37]

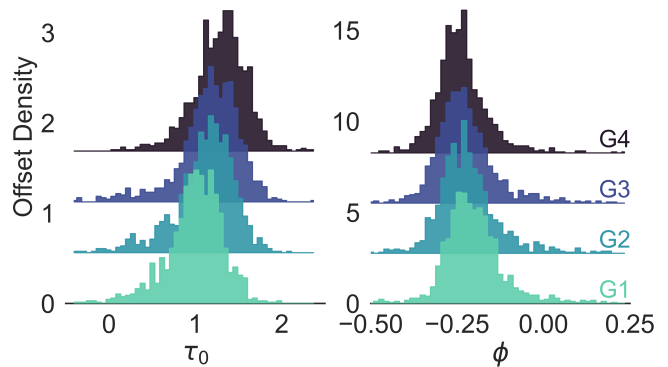


FIG. 2: Distributions of the intrinsic critical stresses τ_0 and pressure dependencies, ϕ , collected from 4 different glasses. The values are colored by quench rate. Each distribution is shifted for clarity. The mean value of τ_0 shifts higher as the cooling rate decreases, while ϕ shows a shift towards lower values at slower cooling rates. See Table I for more detail. Quench rate dependencies of the mean values of τ_0 and ϕ are provided in Figure S1 of the Supplementary Materials.

TABLE I: Summary statistics for the intrinsic critical stress τ_0 and pressure sensitivity ϕ across preparation conditions. Cooling rates are provided in the methods section.

Condition	$\langle \tau_0 \rangle$	s.d.	$\langle \phi \rangle$	s.d.
G1:	1.023 ± 0.009	0.337	-0.196 ± 0.003	0.105
G2:	1.141 ± 0.011	0.372	-0.211 ± 0.004	0.121
G3:	1.192 ± 0.011	0.357	-0.221 ± 0.003	0.091
G4:	1.307 ± 0.009	0.317	-0.230 ± 0.002	0.082

We next test the hypothesis that the positive curvature regions that we find to be well-characterized by Eq. 2 correspond to distinct STZs. Displacement fields are compared to characterize the plastic rearrangements that occur when a sample yields under applied shear. We compute plastic displacement by subtracting the positions of the atoms immediately before and after yielding. In doing so, we subtract the affine displacement imposed due to the shear at the boundary. In Figure 3, seven displacement fields are shown, each corresponding to a fitted minimum. The displacement fields are labelled A-G corresponding to the minima in the bottom half of Figure 1.

Notably, each STZ so identified has a quantifiably similar displacement field throughout its range. For a sample with N atoms, the resulting normalized plastic displacement field is a $2N$ vector \vec{V}_i comprised of the x and y displacements for each atom. The inner product of any two such displacement fields quantifies the degree of sim-

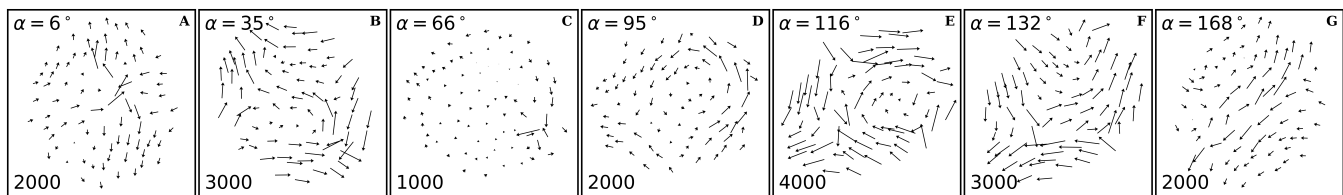


FIG. 3: Plastic displacement fields shown for the regions labeled A-G in Fig. 1(bottom), with their scaling factor in the bottom left. The fields can be easily clustered by direction through similarity using Eq. 3. From Fig. 1(top), each distinct deformation mode can be consistently associated with positive curvature regions throughout its angular domain.

ilarity which can be expressed as a real number $r \in [0, 1]$.

$$r = \frac{\vec{V}_1 \cdot \vec{V}_2}{|\vec{V}_1||\vec{V}_2|} \quad (3)$$

A value of 1 would signify that the two deformation responses were identical, whereas a value of 0 would indicate that the two responses were orthogonal.

The lower panel of Figure 1 applies the metric provided in Eq. 3 to compare the plastic rearrangements triggered by applying shear at different angles to one sampled region. The positive curvature regions in the upper portion of the figure correspond closely with the dark regions in the lower plot. These dark regions denote similarity between the plastic rearrangements triggered at different loading angles. The absence of dark regions off the diagonal suggests that each positive curvature region has a characteristic deformation response not found at any other angle of shear.

To check the consistency of this result among all fitted positive curvature regions in all samples, we compute the median value of similarity within each such region. Our dataset consists of 20, 803 positive-curvature regions across all 4 glasses, previously identified as candidates for fitting. To test our hypothesis without bias from grouping, we consider each candidate region separately. We found statistically significant differences in the variance of the similarity metric across cooling procedures. Thus, we do not group across cooling procedures to assess the similarity. We find that 96.64% of all STZs have a median similarity measure of 90% or higher. This indicates that regions of positive curvature correspond with STZs that undergo markedly similar rearrangements. Panels A–G in Figure 3 show displacement fields at the angle α corresponding to the closest direction to the fitted weak plane direction θ of each STZ. These displacement fields illustrate that distinct STZs exhibit characteristic displacement signatures as quantified using Eq. 3

Discussion— In this study, we address two questions central to linking the STZ concept in amorphous solids to nanoscale plasticity. First, we test whether the nanoscale yield surface can be interpreted as the manifestation of discrete STZ-like entities. Our results show that this

holds for a substantial fraction of the local yield surface in a two-dimensional Lennard–Jones glass. Second, we examine whether the associated plastic rearrangements uniquely characterize the corresponding portions of the yield surface. The data support this connection in the model system considered. We further find that the local yield surfaces display yielding signatures consistent with a combination of Mohr–Coulomb and Schmid-type criteria. This enables a decomposition of the yield surface into a discrete set of segments, each apparently associated with a single STZ. From this decomposition, we can estimate the STZ number density in the glass and quantify how their response depends on both shear orientation and pressure. These findings open a promising route for future investigations that aim to connect atomistic rearrangements to population-based predictive descriptions of glass microstructural evolution during plasticity in amorphous solids.

Acknowledgements— This material is based upon work supported by the U.S. National Science Foundation (DMREF-2323718). This work was carried out at the Advanced Research Computing at Hopkins (ARCH) core facility (rockfish.jhu.edu), which is also supported by the U.S. National Science Foundation (OAC-1920103).

-
- [1] W. L. Johnson, *Bulk Glass-Forming Metallic Alloys: Science and Technology*, Tech. Rep. (1999).
 - [2] W. Klement, W. R. H., and P. O. L. Duwez, Non-crystalline structure in solidified gold–silicon alloys, *Nature* **187**, 869 (1960).
 - [3] C. A. Schuh, T. C. Hufnagel, and U. Ramamurty, Mechanical behavior of amorphous alloys, *Acta Materialia* **55**, 4067 (2007).
 - [4] J. Eckert, J. Das, S. Pauly, and C. Duhamel, Mechanical properties of bulk metallic glasses and composites (2007).
 - [5] A. Nicolas, E. E. Ferrero, K. Martens, and J.-L. Barrat, Deformation and flow of amorphous solids: Insights from elastoplastic models, *Reviews of Modern Physics* **90**, 045006 (2018).
 - [6] D. Rodney, A. Tanguy, and D. Vandembroucq, Modeling the mechanics of amorphous solids at different length scale and time scale, *Modelling and Simulation in Mate-*

- rials Science and Engineering **19**, 083001 (2011).
- [7] A. Argon, Plastic deformation in metallic glasses, *Acta Metallurgica* **27**, 47 (1979).
- [8] F. Spaepen, A microscopic mechanism for steady state inhomogeneous flow in metallic glasses, *Acta Metallurgica* **25**, 407 (1977).
- [9] T. C. Hufnagel, Christopher A. Schuh, and Michael L. Falk., Deformation of metallic glasses: Recent developments in theory, simulations, and experiments., *Acta Materialia* **109**, 375 (2016).
- [10] M. L. Falk and J. S. Langer, Dynamics of viscoplastic deformation in amorphous solids, *Physical Review E* **57**, 7192 (1998).
- [11] A. Phillips and R. Sierakowski, On the concept of the yield surface, *Acta Mechanica* **1**, 29 (1965).
- [12] M. J. Michno Jr and W. N. Findley, An historical perspective of yield surface investigations for metals, *International Journal of Non-Linear Mechanics* **11**, 59 (1976).
- [13] C. A. Schuh and A. C. Lund, Atomistic basis for the plastic yield criterion of metallic glass, *Nature Materials* **2**, 449 (2003).
- [14] R. Hill, *The mathematical theory of plasticity*, Vol. 11 (Oxford university press, 1998).
- [15] F. Lançon, L. Billard, and P. Chaudhari, Thermodynamical properties of a two-dimensional quasi-crystal from molecular dynamics calculations, *Europhysics Letters (EPL)* **2**, 625 (1986).
- [16] F. Leoni, J. Russo, F. Sciortino, and T. Yanagishima, Generating ultrastable glasses by homogenizing the local virial stress, *Phys. Rev. Lett.* **134**, 128201 (2025).
- [17] A. Barbot, M. Lerbinger, A. Hernandez-Garcia, R. García-García, M. L. Falk, D. Vandembroucq, and S. Patinet, Local yield stress statistics in model amorphous solids, *Physical Review E* **97**, 033001 (2018).
- [18] Y. Shi and M. L. Falk, Strain Localization and Percolation of Stable Structure in Amorphous Solids, *Physical Review Letters* **95**, 095502 (2005).
- [19] G. Wahnström, Molecular-dynamics study of a supercooled two-component lennard-jones system, *Physical Review A* **44**, 3752 (1991).
- [20] See Supplemental Material at [URL will be inserted by publisher] for details of the Lennard-Jones cutoff procedure and simulation parameters.
- [21] S. Patinet, D. Vandembroucq, and M. L. Falk, Connecting Local Yield Stresses with Plastic Activity in Amorphous Solids, *Physical Review Letters* **117**, 10.1103/PhysRevLett.117.045501 (2016).
- [22] D. Ruan, S. Patinet, and M. L. Falk, Predicting plastic events and quantifying the local yield surface in 3d model glasses, *Journal of the Mechanics and Physics of Solids* **158**, 104671 (2022).
- [23] D. Richard, M. Ozawa, S. Patinet, E. Stanifer, B. Shang, S. A. Ridout, B. Xu, G. Zhang, P. K. Morse, J.-L. Barrat, L. Berthier, M. L. Falk, P. Guan, A. J. Liu, K. Martens, S. Sastry, D. Vandembroucq, E. Lerner, and M. L. Manning, Predicting plasticity in disordered solids from structural indicators, *Phys. Rev. Mater.* **4**, 113609 (2020).
- [24] C. Maloney and A. Lemaître, Universal breakdown of elasticity at the onset of material failure, *Phys. Rev. Lett.* **93**, 195501 (2004).
- [25] D. L. Malandro and D. J. Lacks, Molecular-level mechanical instabilities and enhanced self-diffusion in flowing liquids, *Phys. Rev. Lett.* **81**, 5576 (1998).
- [26] A. C. Lund and C. A. Schuh, Yield surface of a simulated metallic glass, *Acta Materialia* **51**, 5399 (2003).
- [27] A. Lund and C. Schuh, The mohr–coulomb criterion from unit shear processes in metallic glass, *Intermetallics* **12**, 1159 (2004).
- [28] Y. Zhao, J. Lu, Y. Zhang, F. Wu, and D. Huo, Development of an analytical model based on mohr–coulomb criterion for cutting of metallic glasses, *International Journal of Mechanical Sciences* **106**, 168 (2016).
- [29] M. Lerbinger, *Local shear rearrangements in glassy systems : from micromechanics to structural relaxation in supercooled liquids*, Theses, Université Paris sciences et lettres (2020).
- [30] K. W. Vugrin, L. P. Swiler, R. M. Roberts, N. J. Stucky-Mack, and S. P. Sullivan, Confidence region estimation techniques for nonlinear regression in groundwater flow: Three case studies, *Water Resources Research* **43**, 10.1029/2005WR004804 (2007).
- [31] M. Ozawa, L. Berthier, G. Biroli, A. Rosso, and G. Tarjus, Random critical point separates brittle and ductile yielding transitions in amorphous materials, *Proceedings of the National Academy of Sciences* **115**, 6656 (2018).
- [32] M. Ozawa, L. Berthier, G. Biroli, and G. Tarjus, Role of fluctuations in the yielding transition of two-dimensional glasses, *Physical Review Research* **2**, 023203 (2020).
- [33] A. Barbot, M. Lerbinger, A. Lemaître, D. Vandembroucq, and S. Patinet, Rejuvenation and shear banding in model amorphous solids, *Physical Review E* **101**, 033001 (2020).
- [34] J. Rottler and M. O. Robbins, Unified description of aging and rate effects in yield of glassy solids, *Physical Review Letters* **95**, 225504 (2005).
- [35] G. Yu, J. Lin, M. Mo, X. Wang, F. Wang, and C. Wen, Effect of relaxation on pressure sensitivity index in a zr-based metallic glass, *Materials Science and Engineering: A* **460-461**, 58 (2007).
- [36] G. Yu, J. Lin, and W. Li, A new approach for measuring the pressure sensitivity index of zr-based metallic glasses using indentation tests, *Philosophical Magazine Letters* **90**, 393 (2010).
- [37] A. Dubach, K. E. Prasad, R. Raghavan, J. F. Löffler, J. Michler, and U. Ramamurty, Free-volume dependent pressure sensitivity of zr-based bulk metallic glass, *Journal of Materials Research* **24**, 2697 (2009).

Supplemental Material

S1. SMOOTHED WAHNSTRÖM POTENTIAL (WAHNS)

We use a modified version of the Wahnström binary Lennard–Jones (LJ) glass-forming system [18, 19]. Glass structures are generated following Ref. [15, 17, 18]. The pair potential is given by

$$E(r) = \begin{cases} 4\epsilon \left[\left(\frac{\sigma}{r}\right)^{12} - \left(\frac{\sigma}{r}\right)^6 \right] - E_0, & r < r_{\text{in}}, \\ C_0 - C_1(r - r_{\text{in}}) - \frac{C_2}{2}(r - r_{\text{in}})^2 - \frac{C_3}{3}(r - r_{\text{in}})^3 - \frac{C_4}{4}(r - r_{\text{in}})^4, & r_{\text{in}} < r < r_c, \\ 0, & r > r_c. \end{cases} \quad (4)$$

Here r is the interparticle distance, σ is the LJ length scale, and ϵ is the bond energy. The interaction is truncated at $r_c = 2.5\sigma$ with a smooth polynomial continuation between $r_{\text{in}} = 2\sigma$ and r_c such that the potential and its first two derivatives are continuous. The coefficients E_0 and C_i are fixed accordingly; full expressions are provided in the Supplemental Material of Ref. [16].

S2. LOGARITHMIC DEPENDENCE OF FITTED PARAMETERS ON COOLING RATE

Figure S1 shows the mean values of the fitted parameters τ_0 and ϕ as functions of the cooling rate. In both cases, the data are well described by a logarithmic dependence, with 95% confidence intervals indicated. This behavior is consistent with prior two- and three-dimensional simulations and experimental observations [31–37].

S3. FITTING STATISTICS ACROSS COOLING RATES

Table S1 summarizes the fraction of the yield surface exhibiting positive curvature, the fraction retained for fitting, the total fitted portion of the yield surface, and the average percent error as functions of cooling rate.

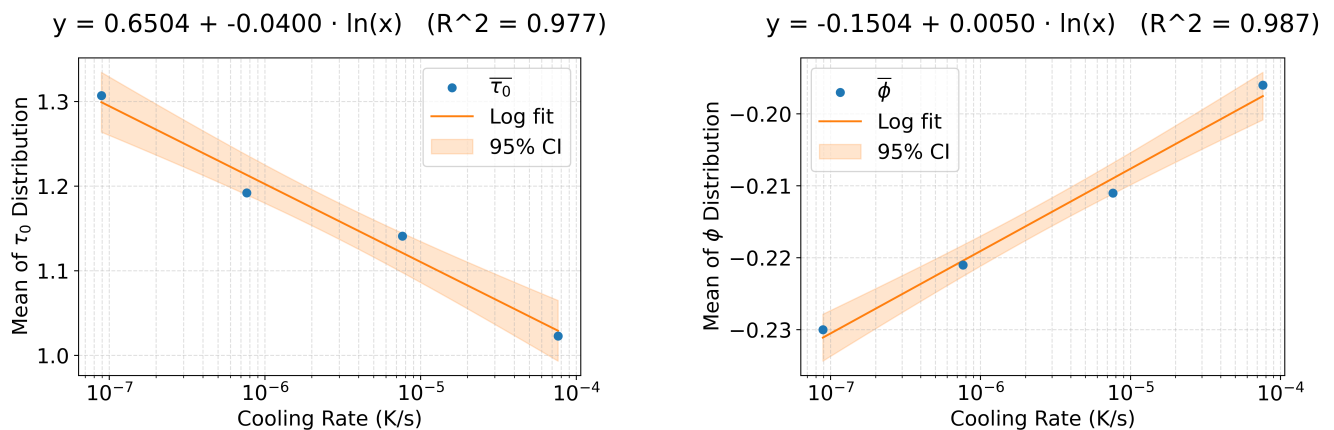


FIG. S1: (a) Mean intrinsic critical stress τ_0 versus cooling rate. (b) Mean pressure sensitivity ϕ versus cooling rate. Shaded regions indicate 95% confidence intervals.

TABLE S1: Fitting statistics across preparation conditions.

Preparation protocol	Convex (% of total)	Kept (% of convex)	Fit (% of total)	Avg. rel. error (%)
G1	69.6	82.1	57.2	2.75
G2	69.5	84.2	58.6	4.93
G3	68.8	84.1	57.9	2.39
G4	69.0	82.8	57.1	2.91